In situ study of the α-Sn to β-Sn phase transition in low-dimensional systems: Phonon behavior and thermodynamic properties

Kelly Houben,[1,*] Johanna K. Jochum,[1,†] Daniel P. Lozano,[2] Manisha Bisht,[2] Enric Menéndez,[2] Daniel G. Merkel,[3,‡] Rudolf Rüffer,[3] Aleksandr I. Chumakov,[3] Sam Roelants,[4] Bart Partoens,[4] Milorad V. Milošević,[4] François M. Peeters,[4] Sebastien Couet,[2] André Vantomme,[2] Kristiaan Temst,[2] and Margriet J. Van Bael[1]

[1]*Laboratory of Solid-State Physics and Magnetism, Celestijnenlaan 200 D, B-3001 Leuven, Belgium*

[2]*Instituut voor Kern- en Stralingsfysica, Celestijnenlaan 200 D, B-3001 Leuven, Belgium*

[3]*European Synchrotron Radiation Facility, F-38043 Grenoble, France*

[4]*Departement Fysica, Universiteit Antwerpen, Groenenborgerlaan 171, B-2020 Antwerpen, Belgium*

(Received 28 March 2017; revised manuscript received 16 July 2019; published 5 August 2019)

The densities of phonon states of thin Sn films on InSb substrates are determined during different stages of the α-Sn to β-Sn phase transition using nuclear inelastic x-ray scattering. The vibrational entropy and internal energy per atom as a function of temperature are obtained by numerical integration of the phonon density of states. The free energy as a function of temperature for the nanoscale samples is compared to the free energy obtained from *ab initio* calculations of bulk tin in the α-Sn and β-Sn phase. In thin films this phase transition is governed by the interplay between the vibrational behavior of the film (the phase transition is driven by the vibrational entropy) and the stabilizing influence of the substrate (which depends on the film thickness). This brings a deeper understanding of the role of lattice vibrations in the phase transition of nanoscale Sn.

DOI: 10.1103/PhysRevB.100.075408

I. INTRODUCTION

Bulk tin undergoes a phase transition at 285 K. The two stable crystalline phases of tin are α-Sn, which is a semiconductor with quasizero band gap, and β-Sn, which is a low-temperature superconductor. α-Sn is stable below 285 K and has a diamond structure, while β-Sn is stable above 285 K and has a body-centered-tetragonal (bct) structure. α-Sn layers can be stabilized at room temperature by heteroepitaxy on a suitable substrate [1]. An α-Sn layer with a thickness up to three monolayers can be stabilized on a Si(111) substrate at room temperature [2,3]. On an InSb(001) substrate ($a = 0.6480$ nm), the stabilization of α-Sn ($a = 0.6489$ nm) at room temperature is possible up to much higher thicknesses (even up to 500 nm [4]) due to the fact that the lattice misfit between α-Sn and InSb (0.14%) is considerably smaller than between α-Sn and Si ($a = 0.5431$ nm; 16%). α-Sn on InSb substrates is referred to as a metastable or a pseudomorphic phase: it is a nonequilibrium phase which is stabilized in epitaxial films because of the lattice-constant matching between α-Sn and InSb and because of a large volume change (28%) between the α-Sn and β-Sn phases [5].

The structural phase transition in tin has received a lot of theoretical [6–11] and experimental [4,12–18] attention. According to theoretical calculations, the phase transition in tin is entropy mediated; that is, above a certain temperature the entropy of the β-Sn phase is large enough to overcome the difference in internal energy between α- and β-Sn, so that β-Sn becomes the stable phase. However, very little information regarding the experimental values of the entropy during the phase transition is available. The experimental studies done so far have determined the phase transition temperature as a function of thickness of the α-Sn films and relied on Raman spectroscopy (which allows a partial phonon density of states to be obtained), scanning electron microscopy, or Auger valence electron spectroscopy [4,12,13]. In this study, the full phonon density of states (PDOS) is determined, using nuclear inelastic x-ray scattering (NIS). The vibrational entropy can be obtained from the measured PDOS. Furthermore, the phase transition temperature for two different thicknesses of α-Sn films is experimentally determined.

The phase transition occurring in tin, from a semiconductor to a metal, also occurs in other semiconductors (e.g., Si and Ge) but at high pressures (several hundreds of kilobars) [19]. The fact that the phase transition in tin takes place in an easily accessible experimental range makes tin the ideal material to study the phase transition from the diamond structure α-Sn phase to the bct structure β-Sn phase.

When the full PDOS of the α- and β-Sn phases is known, the vibrational entropy of both phases can be determined [20]. Here, nuclear inelastic x-ray scattering was employed to determine the PDOS of 10- and 20-nm-thick α-Sn layers stabilized on InSb substrates at different temperatures. From the experimentally obtained PDOS, the free energy per atom F as a function of temperature was extracted. Furthermore, the phonon density of states of bulk tin in the α and β phases was determined from *ab initio* calculations. The free-energy curves $F(T)$, which were inferred from these PDOSs, were compared to the free-energy curves obtained for the Sn thin films. From the experimental data obtained in this work, it was concluded that for bulk Sn as well as for Sn thin films stabilized on an InSb substrate, the α- to β-Sn phase transition

*houben.kelly@gmail.com

†jjochum@frm2.tum.de

‡Present address: Wigner Research Centre for Physics, Konkoly-Thege Miklós út 29-33, Budapest, Hungary.

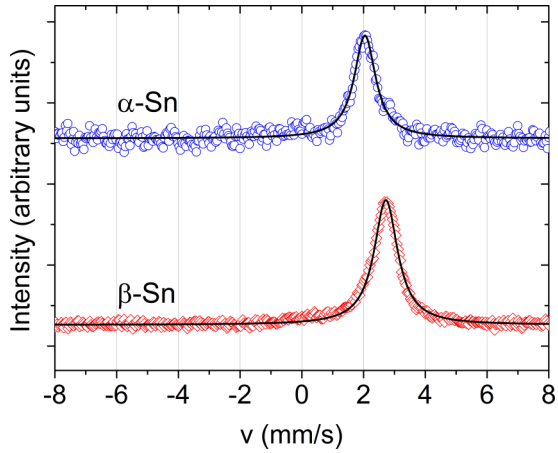

FIG. 1. CEMS measurements of α-Sn (28 nm) and β-Sn (20 nm) thin films, showing the difference in isomer shift between both phases.

is entropy driven. For Sn films deposited on an InSb substrate, the thickness of the layer, rather than the vibrational entropy, determines the temperature at which the phase transition takes place.

II. EXPERIMENTAL AND THEORETICAL TECHNIQUES AND STRUCTURAL CHARACTERIZATION

Sn films were grown on InSb(001) substrates by thermal evaporation in a molecular beam epitaxy (MBE) setup at room temperature. The InSb substrates were cleaned by dipping them for 2 min in a modified CP4A etchant (a mixture of HF, HNO_3, and CH_3COOH [21]) and rinsing them in deionized water for 3 min prior to loading them into the MBE. In vacuum, the surface of the InSb substrates was cleaned by Ar ion bombardment (500 eV Ar ions for 10 min, 1 μA/cm^2) and annealing (at 210 °C for 20 min and at 440 °C for 30 min in a vacuum better than 3×10^{-9} mbar) [4,13,22]. The surface composition after Ar sputtering was checked by Auger electron spectroscopy. The quality of the InSb substrate after the cleaning procedures was checked by reflection high-energy electron diffraction. Isotopically enriched Sn (97% ± 1% ^{119}Sn) was evaporated from a calibrated Knudsen cell at 950 °C at a rate of 0.01 Å/s.

Information on the Sn phase was obtained using conversion electron Mössbauer spectroscopy (CEMS) at room temperature. Due to its Mössbauer-active isotope, ^{119}Sn is suited for Mössbauer spectroscopy. A ^{119m}Sn source (transition energy of 23.87 keV, half-life of 250 days, prepared by neutron capture in isotopically enriched ^{118}Sn) in a $CaSnO_3$ matrix is used with a nominal activity of 10 mCi. The Mössbauer spectra were least squares fitted with the program RECOIL [23] using a Lorentzian line shape. All spectra were recorded at room temperature, and all values of isomer shifts are given with respect to $CaSnO_3$ [24]. In Fig. 1 the results of CEMS measurements of an α-Sn thin film (28 nm) and a β-Sn sample (20 nm) are shown. By fitting the CEMS data with Lorentzian line shapes, the isomer shifts and quadrupole splittings were obtained (see Table I).

TABLE I. Mössbauer parameters of α-Sn/InSb(001) and β-Sn/Si(111) obtained from CEMS measurements at room temperature, compared to the corresponding bulk values reported in the literature.

Sample	Isomer shift δ (mm/s)
8 nm Si/28 nm α-Sn/InSb(001)	2.04 ± 0.04
α-Sn bulk [24,25]	2.02 ± 0.02
20 nm Si/20 nm β-Sn/Si(111)	2.72 ± 0.02
β-Sn bulk [24,25]	2.54 ± 0.01

To structurally characterize the samples, (grazing incidence) x-ray diffraction [(GI)XRD] was carried out (PANalytical X'Pert PRO x-ray diffractometer using Cu $K_{\alpha 1}$ radiation). The incidence angle of the GIXRD measurements was 1°. Information about the lattice parameters and crystallite sizes of the Sn samples were extracted from Rietveld refinements [26] using the MAUD software [27].

XRD measurements were performed on bare InSb substrates, from which it was found that the lattice constant of the InSb substrates ($a = 0.6466$ nm) was slightly smaller than the lattice constant for bulk InSb found in the literature ($a = 0.64798$ nm). This results in an in-plane compressive strain of ≈0.4% of the α-Sn layers compared to bulk α-Sn.

To obtain information on the topography of the samples, atomic force microscope (AFM) images were recorded after the transition from the α-Sn layers to the β-Sn phase in air (Multimode 8 system, Bruker). From the AFM images in Fig. 2 it can be seen that the morphology changes from a flat film for the α-Sn phase to a granular morphology for the β-Sn phase. At the same time the film roughness increases drastically (see Table II). The average heights of the β-Sn

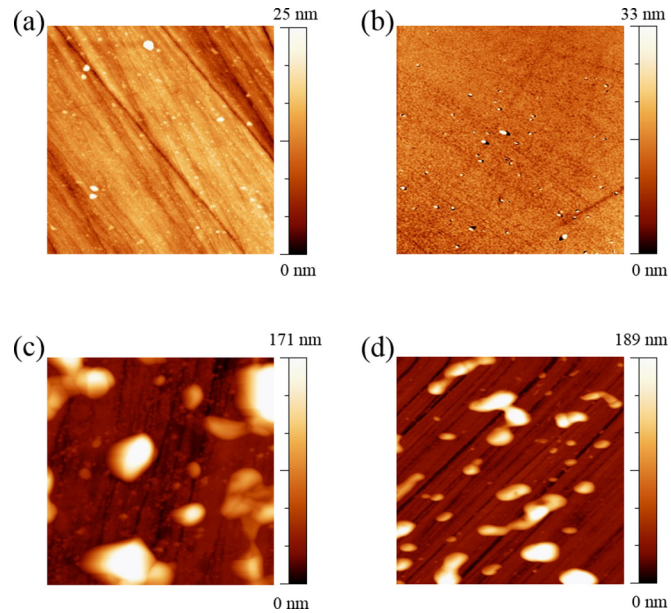

FIG. 2. The $7 \times 7\,\mu$m^2 AFM images of (a) the InSb substrate, (b) 40 nm α-Sn on InSb, (c) 10 nm β-Sn on InSb, and (d) 20 nm β-Sn on InSb [in (c) and (d), thicknesses refer to nominal α-Sn thicknesses].

TABLE II. Nominal thickness and RMS roughness.

Sample	Bare InSb	40 nm α-Sn	10 nm β-Sn	20 nm β-Sn
Nominal Sn thickness (nm)	0	40	10	20
RMS roughness (nm)	2.6 ± 0.6	2.5 ± 0.8 nm	36 ± 3	35 ± 4

grains of the films with nominal α-Sn thicknesses of 10 and 20 nm are very similar: 64 ± 7 and 60 ± 5 nm, respectively. Due to these similarities in grain size and morphology, the PDOS of both samples in the β-Sn phase will not be compared to each other. Rather, the PDOS of the nanostructured samples will be compared to the PDOS of the bulk β-Sn.

The phonon density of states was probed using nuclear inelastic x-ray scattering of synchrotron radiation. The NIS measurements were performed at the Nuclear Resonance beamline (ID-18) at the European Synchrotron Radiation Facility, equipped with a high-resolution monochromator with a resolution of 1 meV [28]. A grazing incidence scattering geometry was employed, and Kirkpatrick-Baez mirrors were used to focus the beam vertically to a size of 9.5 μm, while the lateral size of the beam was 1.5 mm. The samples were prepared and measured *in situ* in the UHV setup at beamline ID-18 [29]. The recipe for growing the α-Sn layers on the InSb substrates was optimized at the Ion and Molecular Beam Laboratory at KU Leuven. NIS measurements were carried out at 110 ± 40 K. The phonon spectra were measured in ultrahigh vacuum (2×10^{-11} mbar) to avoid any oxidation of the prepared samples.

The experimental phonon density of states was complemented by *ab initio* calculations. The phonon density of states of the α-Sn phase was calculated making use of the QUANTUM ESPRESSO density functional theory (DFT) suite. The pseudopotential used was an ultrasoft pseudopotential provided by the QUANTUM ESPRESSO database, constructed within the local-density approximation (LDA). The plane-wave cutoff energy for the electron wave function and charge densities was set to 272 and 1088 eV, respectively. Electron wave functions were sampled on a $5 \times 5 \times 5$ mesh.

The calculations of the phonon density of states of the β-Sn phase were performed using the ABINIT [30] DFT package, using a plane-wave basis and working within the LDA, making use of a Trouiller-Martins pseudopotential [31,32] supplied by the Fritz-Haber Institute. The energy associated with the reciprocal wave vectors was chosen to be 1088 eV (i.e., the plane-wave cutoff energy), and the Brillouin zone is sampled on a regularly spaced $15 \times 15 \times 15$ grid of k vectors. The structure is relaxed to its equilibrium lattice spacing at 0 K, which is found to be $a = 0.568$ nm with cell ratio $c/a = 0.541$. This compares well with the room-temperature result of $a = 0.583$ nm and $c/a = 0.545$ reported in the literature [33].

III. RESULTS AND DISCUSSION

A. Evolution of transition temperature

After α-Sn films were grown on InSb substrates at room temperature, the phase transition from the α- to the β-Sn phase was induced by increasing the temperature. The transition temperature depends on film thickness and is determined by the balance between the layer thickness and the lattice constant mismatch between α-Sn or β-Sn and the InSb substrate [13,34]. The transition temperature from the α to the β phase was determined by monitoring the nuclear resonant elastic time spectra [35] at different temperatures. The temperature at which a change in the time spectrum was observed was defined as the transition temperature. To induce the Sn phase transition in a 20-nm-thick α-Sn film, heating of the sample up to 430 K was required. For the 10-nm-thick α-Sn film, a temperature of 450 K was necessary. A pseudomorphic overlayer ultimately transforms to its stable crystallographic structure when the free energy of the pseudomorphic phase is equal to the free energy of the fully transformed overlayer [36]. The pseudomorphic layer, the α-Sn phase in this case, is strained. From the XRD measurements, a strain of 0.4% is found. As the thickness of the α-Sn layer increases, so does the strain energy E_s in the layer ($E_s \propto h$, with h being the thickness of the layer). At some thickness it becomes energetically favorable to introduce misfit dislocations. The strain energy released by misfit dislocations equals the energy required to form the misfit dislocations. The critical thickness for the introduction of misfit dislocations can be found by minimization of energy: the total energy is the sum of the strain energy and the energy of misfit dislocations [37,38]. Here, a first-order phase transition is considered, which means that at the critical thickness the transition from a strained α-Sn layer to an unstrained β-Sn layer is discontinuous and instantaneous [36] (instead of a thickening layer which gradually releases epitaxial strain by introducing misfit dislocations).

Within the Matthews approximation [39] for the misfit dislocation energy, the thickness dependence of the transition temperature can be found [36,40]. The energy per unit area E_d of a misfit dislocation is proportional to

$$E_d \propto \left[1 + ln\left(\frac{h}{d}\right)\right]. \tag{1}$$

In this equation, h is the thickness of the overlayer, and d is the separation between atomic layers in the direction perpendicular to the sample plane ($d = 0.28$ nm [41]).

The energy associated with the strain E_s in the α-Sn film [36] is

$$E_s \propto h(T_B - T), \tag{2}$$

where T_B is the phase transition temperature in the bulk (= 285 K). The transition temperature as a function of layer thickness h is then given by the following equation:

$$T(h) = 285\,\mathrm{K} - A\frac{1 + ln\left(\frac{h}{0.28}\right)}{h}. \tag{3}$$

In Fig. 3 the phase transition temperature as a function of layer thickness is shown according to Eq. (3)

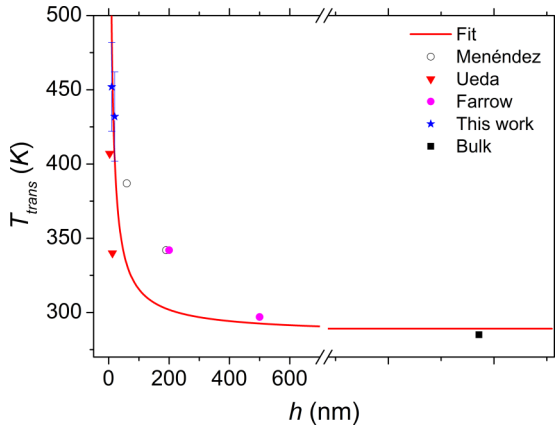

FIG. 3. Phase transition temperature as a function of layer thickness according to Eq. (3) (solid red curve). The blue stars indicate the experimental points found in this work, the open black circles are the data points from Menéndez and Höchst [12], the red triangles are the data points from Ueda *et al.* [13], the magenta circles are the data points from Farrow *et al.* [4], and the black square indicates the bulk value [6].

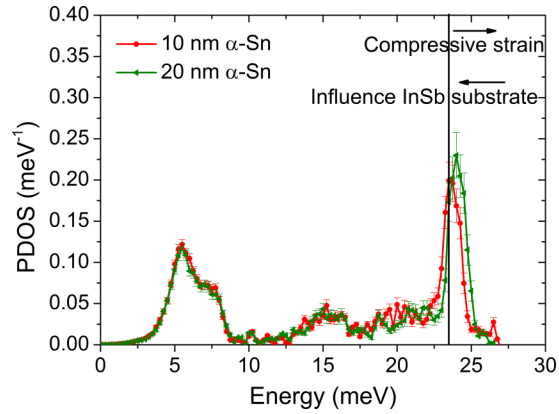

FIG. 4. PDOS of 10 and 20 nm α-Sn (10ph110 and 20ph110). The vertical line indicates the position of the TO peak for bulk α-Sn. The arrows indicate that the TO peak is expected to shift towards higher energies under compressive strain, while the TO peak is expected to shift towards lower energies under the influence of the InSb substrate.

($A = -445.2$ K nm is a fitting parameter). Data points from the literature of α-Sn films on InSb(001) substrates [4,12,13] are shown together with the data points obtained in this study. The bulk value of the transition temperature is also indicated.

Equation (3) is obtained by simple considerations. The presence of an activation barrier against nucleation of such dislocations is not taken into account [34]. Furthermore, this consideration assumes that the transition leads to a single crystal of the transformed material since strain relief through misfit dislocations is considered. In practice, this is, however, not the case: the strain at the interface between the InSb substrate and the layer is typically relieved by formation of twin boundaries, and the bulk stable phase is a mosaic of domains [36]. The polycrystalline nature of the samples in the β-Sn phase is confirmed by XRD measurements (not shown). In the following section, the phonon behavior in the α-Sn and β-Sn phases is discussed.

B. Phonon density of states

1. Phonon density of states in 10- and 20-nm α-Sn layers

Two Sn samples with thicknesses of 10 and 20 nm were prepared, and their PDOS was measured at different stages during the phase transition; see Table III for the different parameters and the sample nomenclature. At or above room temperature, it is very difficult to separate the single-phonon contribution from the multiphonon contributions for β-Sn due to the very low recoilless fraction [14,42]. This is the reason why the samples were cooled down to ≈110 K before measuring the phonon spectrum.

TABLE III. Identification of samples and sample history. For AAphXXX, AA indicates the thickness of the sample, and XXX indicates the temperature up to which the sample was heated.

PDOS measurement	10-nm sample	20-nm sample
PDOS at 110 K	10ph110	20ph110
Heated to 330 K, PDOS at 110 K		20ph330
Heated to 430 K, PDOS at 110 K	10ph430	20ph430
Heated to 450 K, PDOS at 110 K	10ph450	

Figure 4 shows the PDOS of the *in situ* grown 10-nm α-Sn (10ph110) and 20-nm α-Sn (20ph110) films, with typical features of the PDOS of α-Sn: a broad transverse-acoustic peak at low energies (5 meV) and a strong transverse-optical (TO) peak at higher energies (23.5 meV). It can be seen from Fig. 4 that, while the TO peak of 10ph110 coincides with the peak of bulk Sn, the TO peak of 20ph110 is shifted to slightly higher energies. This result may seem counterintuitive at first since it would be expected that the thicker layer would imitate the behavior of a bulk sample more closely. However, as mentioned in Sec. II the films are subject to a small compressive strain of approximately 0.4% due to the lattice mismatch with the InSb substrate. It was shown by Şopu *et al.* that compressive strain results in a shift of the entire PDOS to higher frequencies [43]. Figure 5(a) shows the measured PDOS of sample 20ph110 together with a calculated PDOS of bulk α-Sn with an in-plane compressive strain of 1%. It can be seen that the position of the TO peak of 20ph110 is in good agreement with the calculated PDOS. The TO peak of 10ph110, however, is shifted to slightly lower energies (23.7 meV) than would be expected when taking compressive strain into account (≈24 meV). Considering that both samples were grown under the same conditions on the same substrates (the lattice parameters of which have been determined), both films should be subject to approximately the same amount of strain. Another effect that has been observed in the vibrational behavior of thin films is that the local vibrational properties of a thin film can reflect the vibrational properties of the substrate it has been grown on [44]. Such an effect would be more pronounced in the thinner of the films due to the increase in the surface-to-volume ratio. The TO peak of InSb lies at lower energies than that of α-Sn. The inset in Fig. 5(b) shows the PDOS of InSb (from [45]) together with the calculated

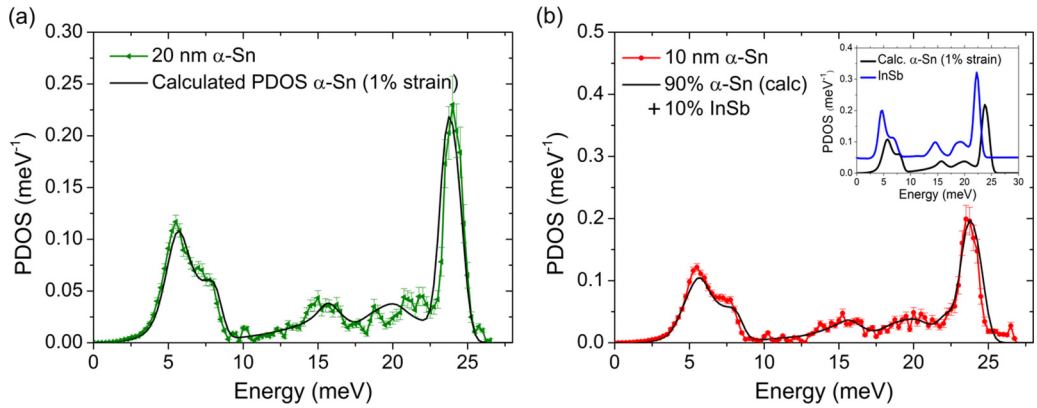

FIG. 5. Phonon density of states of the α-Sn phase. (a) 20ph110 compared to calculated α-Sn PDOS (1% strain); (b) 10ph110 compared to the phonon spectrum consisting of 90% calculated α-Sn (1% strain) and 10% InSb [45]. The inset shows the PDOS of the InSb substrate (shifted vertically for the sake of clarity by 0.05 meV) and the PDOS of strained α-Sn.

PDOS of α-Sn. In Fig. 5(b), 10ph110 is plotted together with a PDOS composed of 90% of the calculated PDOS of strained α-Sn and 10% PDOS of InSb. This ratio of α-Sn and InSb showed the best agreement with the experimentally obtained 10ph110 PDOS. It can be concluded that the vibrational behavior of the α-Sn atoms in the 10-nm layer is influenced by two effects: compressive strain and the coupling to the vibrational behavior of the InSb substrate.

2. *Phonon density of states for 10- and 20-nm samples during the temperature-induced α-Sn to β-Sn phase transition*

After the PDOSs for the 10- and 20-nm samples in the α-Sn phase were measured at 110 K, the structural phase transition in these samples was induced by raising the temperature. Time spectra were recorded at regular intervals while increasing the temperature. After the desired temperature was reached, the samples were brought back to 110 K for the PDOS measurement.

Three phonon spectra were measured for each sample, as shown in Figs. 6(a) and 6(b). The upper PDOS represents the sample in the α-Sn phase, while the lower spectrum is the PDOS of the sample in the β-Sn phase. The reduced range of vibrational energies in the β-Sn phase compared to the α-Sn phase can be clearly observed.

In Fig. 6(a), a small peak can be seen at 23.5 meV in 10ph450 (indicated by the arrow), the exact position of the TO peak in α-Sn. This indicates that the 10-nm sample is not yet fully transformed into the β-Sn phase after heating up to 450 K and that approximately 10% of the 10-nm sample is still in the α-Sn phase. The 20-nm sample, however, is fully transformed to the β-Sn phase after heating to 430 K.

It should be mentioned that the TO peak of 10ph430 in Fig. 6(a) is shifted to higher energies compared to that of 10ph110. The TO peak of 10ph430 is at the same position as the peak of 20ph110 and 20ph330. A possible explanation could be that as the temperature increases and the phase transition is approached, the film gets decoupled from the substrate and the vibrational properties of the substrate do not play such a strong role in the PDOS of the film anymore. To fully explore the shift in the TO peak resulting from compressive strain as well as the effects of the substrate, a dedicated, systematic study should be conducted, which is beyond the scope of this work.

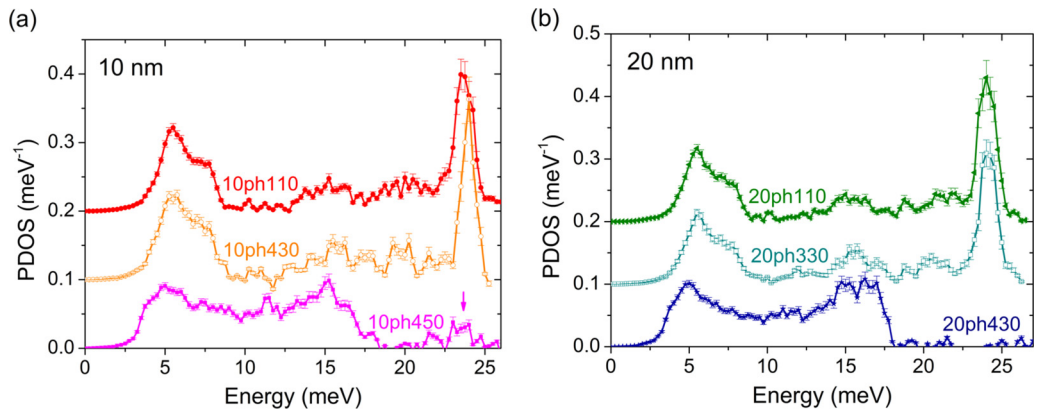

FIG. 6. (a) Evolution in the PDOS during the phase transition in the 10-nm Sn sample. The measurements are performed with the sample at 110 K without prior annealing (top), after annealing at 430 K (middle), and after annealing at 450 K (bottom). The arrow indicates the presence of a small peak attributed to a small fraction of the sample that is still in the α-Sn phase. (b) Evolution in the PDOS during the phase transition in the 20-nm Sn sample. The measurements are performed with the sample at 110 K, without prior annealing (top), after annealing at 330 K (middle), and after annealing at 430 K (bottom).

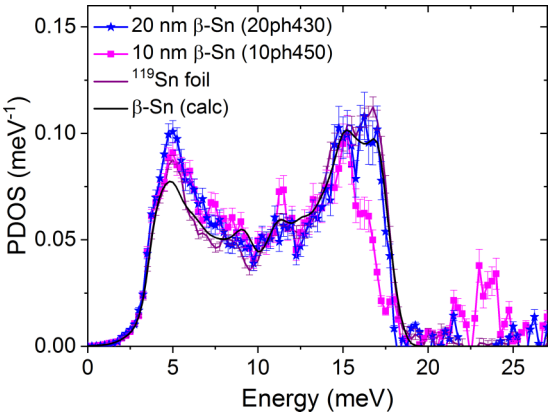

FIG. 7. Phonon density of states of the 10- and 20-nm samples recorded at 110 K after transition to the β-Sn phase (20ph430 and 10ph450), compared to the phonon density of states of bulk β-Sn.

3. Phonon density of states in the β Sn phase

In Fig. 7, 10ph450 and 20ph430 are compared with the measured PDOS of a β-Sn reference foil. A reduction of the intensity of the high-energy phonon modes (17 meV) can be observed in 10ph450 compared to 20ph430 and the ^{119}Sn foil. There are many possible reasons for this reduction in intensity. Confinement effects and phonon damping [44,46–49] have been known to cause a reduction in high-energy phonon modes. Another possibility could be the influence of the InSb substrate, which does not have any modes at 16.3 meV. Since no significant difference in grain size and morphology is seen between 10ph450 and 20ph430, we do not believe that confinement effects can explain the obvious difference between the two PDOSs.

Further, it can be observed from Fig. 7 that 10ph450 is not yet fully converted to the β phase (a small peak corresponding to α-Sn is still present at 23.5 meV). A detailed comparison of the thin film and bulk β-Sn samples is complex due to the very heterogeneous morphology of the thin-film samples and is outside the scope of this study. However, in general we observe that also in the lower-energy range (5.5–8 meV) the phonon mode intensity of 10ph450 and 20ph430 is enhanced compared to the bulk. This increase in low-energy modes indicates that the interatomic interaction is, on average, weaker than in the bulk [50], probably as a consequence of the increased surface area and large number of grain boundaries.

C. Thermodynamic quantities

The transition between two phases occurs when their free energies are equal. The free energy of the α-Sn and β-Sn phases can be determined based on the mean internal energy and the entropy:

$$F = E_{\text{stat}} + U_{\text{int}} - TS, \tag{4}$$

where F is the free energy per atom, E_{stat} is the static lattice energy per atom, U_{int} is the mean internal energy per atom, and S is the entropy per atom. From the phonon density of states measured in both Sn phases, the vibrational entropy per atom S and the mean internal energy per atom U_{int} were calculated [20].

TABLE IV. Thermodynamical properties extracted from the phonon density of states at 110 K. In the second column, the phase of the sample is indicated, as extracted from the measured PDOS (see text). S is the vibrational entropy per atom, U_{int} is the mean internal energy per atom, f_{LM} is the Lamb-Mössbauer factor, $\langle u^2 \rangle$ is the mean-square atomic displacement, C is the specific heat, and B is the mean force constant. The indicated errors are based on the statistical errors on the PDOS.

Sample	Phase	S (k_B)	U_{int} (meV)	f_{LM}
10ph110	α	2.5 ± 0.2	35 ± 5	0.46 ± 0.03
10ph430	α (+ β)	2.6 ± 0.3	35 ± 5	0.42 ± 0.03
10ph450	(α+)β	3.1 ± 0.2	32 ± 2	0.36 ± 0.02
20ph110	α	2.4 ± 0.3	36 ± 5	0.49 ± 0.04
20ph330	α (+ β)	2.3 ± 0.2	37 ± 4	0.50 ± 0.03
20ph430	β	3.2 ± 0.3	32 ± 3	0.36 ± 0.03
β-Sn foil	β	2.9 ± 0.1	32 ± 2	0.41 ± 0.02
Sample	$\langle u^2 \rangle$ (pm^2)	B (N/m)	C (k_B)	
10ph110	54 ± 4	131 ± 20	2.4 ± 0.3	
10ph430	59 ± 5	122 ± 20	2.4 ± 0.3	
10ph450	69 ± 4	70 ± 5	2.6 ± 0.2	
20ph110	49 ± 5	148 ± 21	2.3 ± 0.3	
20ph330	48 ± 6	152 ± 18	2.3 ± 0.3	
20ph430	70 ± 5	60 ± 6	2.7 ± 0.2	
β-Sn foil	61 ± 3	69 ± 3	2.6 ± 0.1	

Furthermore, the Lamb-Mössbauer factor f_{LM}, mean-square atomic displacement $\langle u^2 \rangle$, the specific heat C, and the mean force constant B were obtained. Table IV displays the values of these quantities for both samples, derived from the different measured PDOSs. The difference in entropy between the α and β phases ΔS of $0.6\,k_B$ and $0.8\,k_B$ for the 10- and 20-nm films, respectively, agrees very well with what has been found previously ($0.68\,k_B$ [51,52]).

The value of B for 20ph110 (and 20ph330) is similar to that of a 200-nm α-Sn/CdTe film, $B = 155 \pm 16$ N/m (which is considered an α-Sn bulk reference) [14]. There is a tendency for B to be slightly lower in the 10-nm α-Sn samples (10ph110 and 10ph430). This can be attributed to the influence of the InSb substrate (see also Fig. 5), which has a significantly lower force constant than that of α-Sn [53].

As mentioned in Sec. III B 3 both β-Sn thin films show an increase in low-energy phonon mode intensities. This is reflected in the value of B for the thin films, which is slightly lower than for bulk. The fact that approximately 10% of 10ph450 is still in the α-Sn phase explains why the mean force constant of 10ph450 is slightly higher than for 20ph430. The PDOSs which were measured after annealing at intermediate temperatures (10ph430 and 20ph330) as well as the thermodynamic properties derived from them show close resemblance to the α-Sn case.

D. Free-energy curves: Temperature dependence of free energy

From Table IV it can be seen that the mean internal energy per atom U_{int} for the α-Sn phase is systematically higher than for the β-Sn phase at 110 K. When calculating the free energy per atom F as a function of temperature for the α- and β-Sn phases, the difference in static lattice energy between

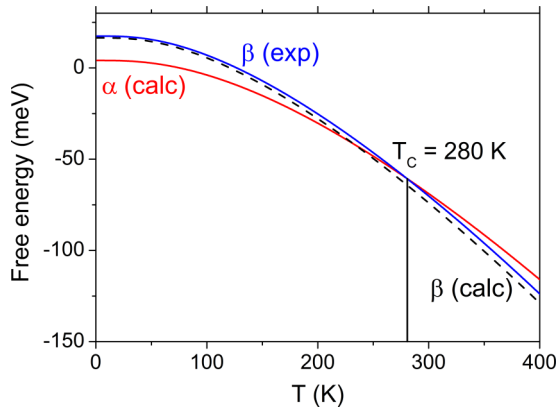

FIG. 8. Free energy F curves for the α-Sn and β-Sn (bulk) phases as a function of temperature. The red solid line and the black dashed line correspond to the free-energy curves obtained by numerical integration of the calculated PDOS for α-Sn and β-Sn, respectively. The blue solid line corresponds to the free-energy curve obtained by numerical integration of the experimentally determined PDOS of a reference β-Sn foil.

the α-Sn and β-Sn polymorphs ($\Delta E_{\text{stat}} = 12.4$ meV/atom) is taken into account. This causes the free-energy curve of the β-Sn phase to be higher than that of the α-Sn phase for temperatures below the phase transition temperature. The vibrational entropy in the β-Sn phase is larger than for the α-Sn phase. This is related to the overall lower vibrational frequencies, especially the optical modes, of the β-Sn PDOS in comparison to the α-Sn PDOS [7].

The measured and calculated PDOSs were numerically integrated to obtain the mean internal energy per atom and the vibrational entropy per atom as a function of temperature. From these, the free energy per atom was calculated as a function of temperature using $F = E_{\text{stat}} + U_{\text{int}} - TS$. The difference in static energy between the two phases, $\Delta E_{\text{stat}} = 12.4$ meV/atom, was obtained from standard local-density-functional calculations. The value agrees well with previous studies ($\Delta E_{\text{stat}} = 15.6$ meV/atom [6], $\Delta E_{\text{stat}} = 15$ meV/atom [10]). Figure 8 shows the free energy extracted from the calculated PDOS for α- and β-Sn as well as the free energy for the measured Sn foil. The excellent agreement between F_β(calc) and F_β(exp) proves that the Sn foil makes an appropriate bulk reference. The curves for F_α(calc) and F_β(calc) cross at the phase transition temperature $T_C = 280$ K, which is close to the experimentally observed value of 285 K. The latent heat observed during the transition is equal to the difference in internal energy at T_C, ΔU_{int}, and was found to be equal to 18.5 meV/atom, close to values reported in the literature [6,10,51,52].

The free-energy curves for the Sn thin films are shown in Fig. 9. The difference in free energy at 0 K is determined by fixing the transition temperature at the experimentally observed temperatures for both samples. For the 10-nm sample $\Delta F(0\,\text{K}) = 25.6$ meV/atom, and for the 20-nm sample $\Delta F(0\,\text{K}) = 28.9$ meV/atom. $\Delta F(0\,\text{K})$ is larger for both nanoscale samples than for the bulk [$\Delta F_{\text{bulk}}(0\,\text{K}) = 12.4$ meV/atom]. For the bulk case, $\Delta F(0\,\text{K}) = \Delta E_{\text{stat}}$. For the nanoscale case, $\Delta F(0\,\text{K})$ has an additional contribution coming from the difference in energy between the introduction of a misfit dislocation and a strained α-Sn layer [$E_d - E_s$; see Eqs. (1) and (2)].

The latent heat per atom absorbed during the α- to β-Sn transition amounts to 35.4 meV for the 20-nm sample and to 30.2 meV for the 10-nm sample and is higher in the thin films compared to the bulk. This is consistent with the fact that the stabilizing influence of the substrate needs to be overcome in the nanoscale samples in order to complete the transition to the β-Sn phase. Despite the similar phonon behaviors of both samples, a clear difference in transition temperature has been observed in the *in situ* NIS experiments.

IV. CONCLUSIONS

The structural phase transition in Sn thin films was studied using nuclear inelastic resonant x-ray scattering and *ab initio* calculations. The NIS technique allows us to probe the full phonon density of states of low-dimensional samples from which important thermodynamic quantities were determined. By numerical integration of the calculated or experimentally determined PDOS, the mean internal energy and the vibrational entropy per atom as a function of temperature were determined. A phase transition temperature of 280 K and a

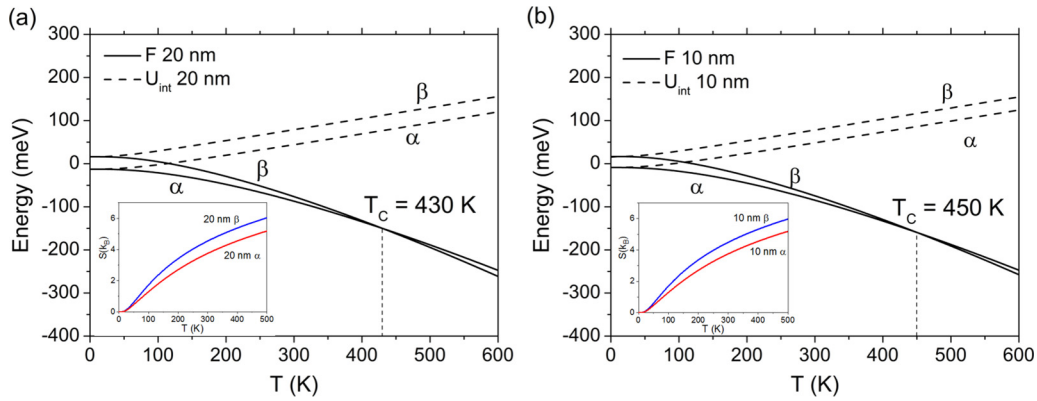

FIG. 9. Energy curves for the α and β phases of Sn as a function of temperature, obtained by numerical integration of the experimentally obtained phonon spectra. (a) The 20-nm sample; (b) the 10-nm sample. The insets show the vibrational entropy/atom as a function of temperature for both Sn phases.

latent heat per atom of 18.5 meV were obtained for bulk Sn (comparable to 21 meV reported earlier [6,10]). From the free-energy curves of bulk Sn, it was concluded that the phase transition from the α-Sn to β-Sn phase occurs due to a stronger increase of the vibrational entropy per atom as a function of temperature for the β-Sn phase compared to the α-Sn phase.

The PDOSs of a 10- and a 20-nm α-Sn film, stabilized at room temperature on an InSb substrate, were measured *in situ* at different stages during the phase transition to the β-Sn phase. It was found that although the difference in phonon behavior between both samples is relatively small, the transition temperature differs significantly (difference of 20 K). The layer thickness determines the energy difference between a strained α-Sn layer and the introduction of a misfit dislocation, which leads to the β-Sn phase. The α-Sn to β-Sn phase transition in thin films is therefore understood as the interplay between the vibrational behavior of the layer (the phase transition is driven by the vibrational entropy) and the stabilizing influence of the substrate (which is dependent on the thickness of the layer). While the vibrational entropy per atom (determined by the phonon behavior) makes the phase transition happen, it is the *thickness* of the α-Sn layer which determines at what temperature the phase transition will happen.

ACKNOWLEDGMENTS

This work was supported by the Research Foundation Flanders (FWO) and the Concerted Research Action (Grant No. GOA14/007). K.H., S.C., D.P.L., and E.M. wish to thank the FWO for financial support. The authors gratefully acknowledge the European Synchrotron Radiation Facility (ESRF) for the granted beam time and the use of the *in situ* UHV preparation chamber. The authors thank B. Opperdoes for technical support and T. Peissker and R. Lieten for fruitful discussions.

[1] H. Brune and K. Kern, Chem. Phys. Solid Surf. **8**, 149 (1997).
[2] D. T. Wang, N. Esser, M. Cardona, and J. Zegenhagen, Surf. Sci. **343**, 31 (1995).
[3] B. R. Cuenya, M. Doi, and W. Keune, Surf. Sci. **506**, 33 (2002).
[4] R. F. C. Farrow, D. S. Robertson, G. M. Williams, A. G. Cullis, G. R. Jones, I. M. Young, and P. N. J. Dennis, J. Cryst. Growth **54**, 507 (1981).
[5] W. A. Jesser, Mater. Sci. Eng. **4**, 279 (1969).
[6] P. Pavone, S. Baroni, and S. de Gironcoli, Phys. Rev. B **57**, 10421 (1998).
[7] S. Na and C. Park, J. Korean Phys. Soc. **56**, 494 (2010).
[8] D. L. Price and J. M. Rowe, Solid State Commun. **7**, 1433 (1969).
[9] R. Ravelo and M. Baskes, Phys. Rev. Lett. **79**, 2482 (1997).
[10] J. Ihm and M. L. Cohen, Phys. Rev. B **23**, 1576 (1981).
[11] M. Boström, M. Dou, O. I. Malyi, P. Parashar, D. F. Parsons, I. Brevik, and C. Persson, Phys. Rev. B **97**, 125421 (2018).
[12] J. Menéndez and H. Höchst, Thin Solid Films **111**, 375 (1984).
[13] K. Ueda, H. Nakayama, M. Sekine, and H. Fujita, Vacuum **42**, 547 (1991).
[14] J. A. Gómez, D. Guenzburger, D. E. Ellis, M. Y. Hu, E. E. Alp, E. M. Baggio-Saitovitch, E. C. Passamani, J. B. Ketterson, and S. Cho, Phys. Rev. B **67**, 115340 (2003).
[15] B. Mason and B. R. Williams, Surf. Sci. **273**, L472 (1992).
[16] A. Skwarek, P. Zachariasz, J. Żukrowski, B. Synkiewicz, and K. Witek, Mater. Chem. Phys. **182**, 10 (2016).
[17] P. Zachariasz, A. Skwarek, B. Illés, J. Żukrowski, T. Hurtony, and K. Witek, Microelectron. Reliab. **82**, 165 (2018).
[18] B. Cornelius, S. Treivish, Y. Rosenthal, and M. Pecht, Microelectron. Reliab. **79**, 175 (2017).
[19] R. W. Smith, J. Less-Common Met. **114**, 69 (1985).
[20] A. I. Chumakov and W. Sturhahn, Hyperfine Interact. **123**, 781 (1999).
[21] W. K. Liu, W. T. Yuen, and R. A. Stradling, J. Vacuum Sci. Technol. B **13**, 1539 (1995).
[22] B. F. Mason and B. R. Williams, Surf. Sci. **262**, 169 (1992).
[23] D. G. Rancourt and J. Y. Ping, Nucl. Instrum. Methods Phys. Res., Sect. B **58**, 85 (1991).
[24] J. G. Stevens, Hyperfine Interact. **13**, 221 (1983).
[25] A. Svane, N. E. Christensen, C. O. Rodriguez, and M. Methfessel, Phys. Rev. B **55**, 12572 (1997).
[26] R. A. Young, Cryst. Res. Technol. **30**, 494 (1995).
[27] L. Lutterotti, S. Matthies, and H. R. Wenk, IUCr Newsl. CPD **21**, 14 (1999).
[28] A. I. Chumakov, A. Barla, R. Rüffer, J. Metge, H. F. Grünsteudel, H. Grünsteudel, J. Plessel, H. Winkelmann, and M. M. Abd-Elmeguid, Phys. Rev. B **58**, 254 (1998).
[29] R. Rüffer and A. I. Chumakov, Hyperfine Interact. **97**, 589 (1996).
[30] X. Gonze, B. Amadon, P. M. Anglade, J. M. Beuken, F. Bottin, P. Boulanger, F. Bruneval, D. Caliste, R. Caracas, M. Côté, T. Deutsch, L. Genovese, P. Ghosez, M. Giantomassi, S. Goedecker, D. R. Hamann, P. Hermet, F. Jollet, G. Jomard, S. Leroux, M. Mancini, S. Mazevet, M. J. T. Oliveira, G. Onida, Y. Pouillon, T. Rangel, G. M. Rignanese, D. Sangalli, R. Shaltaf, M. Torrent, M. J. Verstraete, G. Zerah, and J. W. Zwanziger, Comput. Phys. Commun. **180**, 2582 (2009).
[31] N. Troullier and J. L. Martins, Phys. Rev. B **43**, 1993 (1991).
[32] M. Fuchs and M. Scheffler, Comput. Phys. Commun. **119**, 67 (1999).
[33] N. W. Ashcroft and D. Mermin, *Solid State Physics* (Saunders, Philadelphia, 1976).
[34] A. Zunger and D. M. Wood, J. Cryst. Growth **98**, 1 (1989).
[35] R. Röhlsberger, in *Nuclear Condensed Matter Physics with Synchrotron Radiation* (Springer, Berlin, 2004), pp. 67–100.
[36] R. Bruinsma and A. Zangwill, J. Phys. **47**, 2055 (1986).
[37] J. E. Ayers, *Heteroepitaxy of Semiconductors: Theory, Growth, and Characterization* (CRC Press, Boca Raton, FL, 2007).
[38] E. A. Fitzgerald, Mater. Sci. Rep. **7**, 87 (1991).
[39] J. W. Matthews, J. Vac. Sci. Technol. **12**, 126 (1975).
[40] V. D. Das and D. Karunakaran, J. Phys. Chem. Solids **46**, 551 (1985).

[41] A. D. Styrkas, Inorg. Mater. **39**, 806 (2003).
[42] A. Barla, R. Rüffer, A. I. Chumakov, J. Metge, J. Plessel, and M. M. Abd-Elmeguid, Phys. Rev. B **61**, R14881 (2000).
[43] D. Şopu, J. Kotakoski, and K. Albe, Phys. Rev. B **83**, 245416 (2011).
[44] S. Stankov, R. Röhlsberger, T. Ślęzak, M. Sladecek, B. Sepiol, G. Vogl, A. I. Chumakov, R. Rüffer, N. Spiridis, J. Łażewski, K. Parliński, and J. Korecki, Phys. Rev. Lett. **99**, 185501 (2007).
[45] J. M. Rowe, R. M. Nicklow, D. L. Price, and K. Zanio, Phys. Rev. B **10**, 671 (1974).
[46] S. Couet, H. Peelaers, M. Trekels, K. Houben, C. Petermann, M. Y. Hu, J. Y. Zhao, W. Bi, E. E. Alp, E. Menéndez, B. Partoens, F. M. Peeters, M. J. Van Bael, A. Vantomme, and K. Temst, Phys. Rev. B **88**, 045437 (2013).
[47] R. Röhlsberger, W. Sturhahn, T. S. Toellner, K. W. Quast, P. Hession, M. Y. Hu, J. Sutter, and E. E. Alp, J. Appl. Phys. **86**, 584 (1999).
[48] J. Łażewski, J. Korecki, and K. Parlinski, Phys. Rev. B **75**, 054303 (2007).
[49] T. Ślęzak, J. Łażewski, S. Stankov, K. Parlinski, R. Reitinger, M. Rennhofer, R. Rüffer, B. Sepiol, M. Ślęzak, N. Spiridis, M. Zajac, A. I. Chumakov, and J. Korecki, Phys. Rev. Lett. **99**, 066103 (2007).
[50] P. P. Parshin, M. G. Zemlyanov, G. K. Panova, A. A. Shikov, Y. A. Kumzerov, A. A. Naberezhnov, I. Sergueev, W. Crichton, A. I. Chumakov, and R. Rüffer, J. Exp. Theor. Phys. **114**, 440 (2012).
[51] F. Seitz, *The Modern Theory of Solids* (McGraw-Hill, New York, 1940).
[52] F. Lange, Z. Phys. Chem. **110A**, 343 (1924).
[53] V. Kumar, J. Phys. Chem. Solids **61**, 91 (2000).